Available online at www.sciencedirect.com
SCIENCE DIRECT®
Journal of Solid State Chemistry 179 (2006) 362–369
JOURNAL OF SOLID STATE CHEMISTRY
www.elsevier.com/locate/jssc

Relationship between transport properties and phase transformations in mixed-conducting oxides

Z.Q. Deng[a,*], W.S. Yang[a], W. Liu[b], C.S. Chen[b]

[a]State Key Laboratory of Catalysis, Dalian Institute of Chemical Physics, Chinese Academy of Sciences, Dalian 116023, PR China
[b]Laboratory of Advanced Functional Materials and Devices, Department of Materials Science and Engineering, University of Science and Technology of China, Hefei, Anhui 230026, PR China

Received 14 June 2005; received in revised form 10 October 2005; accepted 20 October 2005
Available online 22 November 2005

Abstract

To elucidate the relationship between transport properties and phase transformations in mixed-conducting oxides, $Sr_{0.9}Ca_{0.1}Co_{0.89}Fe_{0.11}O_{3-\delta}$ (SCCFO) and $SrCoO_{3-\delta}$ (SCO) were chosen as the model materials and have been investigated in detail. Oxygen permeation measurements verified that both oxides are well permeable to oxygen at elevated temperatures, e.g., at 900 °C during a cooling procedure, oxygen permeation rates as large as 1.5 and 2.0 mL/min/cm^2 could be obtained with disk-shaped SCCFO and SCO membranes of thickness 1.5 mm, respectively. But when cooled to critical temperatures, the oxygen permeability of these kinds of oxides diminished sharply, which could be recovered by increasing the temperature again to certain values. Abrupt changes on electrical conductivity were also observed for both oxides around the same region of temperature as that of oxygen permeability. As indicated by high-temperature X-ray diffraction and thermal analysis, the SCCFO and SCO systems undergo phase transformation between a low-temperature orthorhombic brownmillerite structure (B) or a hexagonal 2H-type structure (H) and a high-temperature cubic perovskite structure (C), respectively. The present results suggest the observed abrupt changes in transport properties versus temperature are attributed to such phase transformation, which may be directly associated with the order–disorder transition of oxygen vacancies. Moreover, compared to the B/C transformation that mainly involves an order–disorder transition on the oxygen sublattice, the H/C one necessarily also involves the cooperative long-range reorganization on the cation sublattice. Therefore it occurs at a higher temperature and absorbs more heat quantity than those of B/C transformation.

Keywords: Mixed–conducting oxides; Phase transformation; Order–disorder transition; Electrical conductivity; Oxygen permeability; High-temperature X-ray diffraction

1. Introduction

One of the salient features of some perovskite-type and related oxides $ABO_{3-\delta}$ (A = La, Sr, Ba; B = Co, Fe, etc.) is their large ability to accommodate a wide range of oxygen deficiency and mixed oxidation states of B-site transition metal. By counter-transport of oxide ions via jumping of oxygen vacancies and electrons along the $B^{n+} - O^{2-} - B^{(n-1)+}$ network that is formed through covalent overlapping between B-3d and O-2p orbital, these oxides can be endowed with simultaneous oxide–ion and electronic conduction [1–3]. Accordingly, such oxides hold much promise for use as oxygen separation membranes, methane conversion reactors, and solid oxide fuel cell (SOFC) cathodes [1,4,5].

It is well established [1,6,7] that when the bulk transport process is rate determining for a given mixed conductor, the oxygen flux through a membrane can be expressed in terms of the Wagner equation:

$$j_{O_2} = \frac{RT}{16F^2L}\int_{\ln p''_{O_2}}^{\ln p'_{O_2}} \frac{\sigma_{ion}\sigma_{el}}{\sigma_{ion}+\sigma_{el}}\, d\ln p_{O_2}, \quad (1)$$

where L is the membrane thickness, σ_{el} and σ_{ion} are the electronic and ionic conductivities, and the rest have their usual meaning. In many of the oxides that have been investigated till now, σ_{el} is usually several orders of

*Corresponding author.
E-mail address: dzqm@dicp.ac.cn (Z.Q. Deng).

0022-4596/$ - see front matter © 2005 Elsevier Inc. All rights reserved.
doi:10.1016/j.jssc.2005.10.027

magnitude larger than σ_{ion}; this is also valid for the materials in this work (see below). Thus, Eq. (1) can be simplified to

$$j_{O_2} = \frac{RT}{16F^2L}\int_{\ln p''_{O_2}}^{\ln p'_{O_2}} \sigma_{ion}\, d\ln p_{O_2}. \quad (2)$$

Accordingly, given that the same thickness and oxygen partial pressure gradient are applied, the oxygen flux across a membrane material is determined intrinsically by its ionic conductivity σ_{ion}. From the crystal structure consideration, $SrCoO_{3-\delta}$ (designated as SCO) has long been expected to possess high oxygen permeability, because nearly one-sixth of its oxygen lattice position is unoccupied and the strength of Co–O bond is relatively weak, favoring the transport of oxide ions and electrons [3,8]. However, appreciable oxygen permeability for SCO can only be achieved at elevated temperatures. Upon cooling to certain critical temperatures, it becomes oxygen non-permeable, concomitant with a transition from a high-temperature structure to a low-temperature one [6,9–11]. In this regard, SCO is a case in point for the study of the relationship between transport properties and phase transformation in mixed conductors. On the other hand, one may predict that the oxygen permeability (essentially the oxide–ion conductivity) of mixed-conducting oxides is crucially dependent on the distribution of oxygen vacancies; this has already been well understood in many solid oxide electrolytes. For instance, $Ba_2In_2O_5$ adopt a crystal structure of brownmillerite with an ordered arrangement of oxygen vacancies and ideal perovskite with random distribution of oxygen vacancies below and above ~910 °C, respectively. Corresponding to that order–disorder transition, a significant jump in oxide–ion conductivity was observed [12–14]. Similarly, a mixed conductor with a brownmillerite structure is also expected to show abrupt change in the oxygen permeability versus temperature, which can give distinct clues to effect of the order–disorder transition of oxygen vacancies on oxide–ion transport in such oxides. For this, synthesis of these kinds of oxides is strongly desired.

Knowledge of the relationship between transport properties and phase transformations in mixed conductors is of interest from a technical point of view. It can also provide better insights into implications for ionic and electronic conduction in solids. However, not much information regarding this is available. In the present work, we have undertaken a detailed study of the oxygen permeation and electrical conductivity properties with relation to phase transformation in two novel model materials, $Sr_{0.9}Ca_{0.1}Co_{0.89}Fe_{0.11}O_{3-\delta}$ (designated as SCCFO) and $SrCoO_{3-\delta}$ (SCO). A clear correlation between properties and structure has been well elucidated.

2. Experimental

Samples of SCCFO and $SrCoO_{3-\delta}$ were prepared by a solid-state reaction method. Required quantities of $SrCO_3$ (>99.0%), Fe_2O_3 (>99.0%), and Co_3O_4 (>99.0%) were mixed, ground, and calcined in air for a long time with intermediate grinding. The resulting powders were pressed at 300 MPa into disks and bars. These compacts were sintered at 1150 °C (for SCO) or 1200 °C (for SCCFO) for 8 h and cooled to 500 °C at a rate of 60 °C/h and then furnace cooled to room temperature. X-ray diffraction analysis was carried out on powder samples (Rigaku; RINT-2000, Cu$K\alpha$) at desired higher temperatures with a heating rate of 5 °C/min from room temperature. Each recording took 15 min after a 30 min equilibration. TG/DTA measurement (Pyris Diamond TG/DTA analyzer; Seiko Instrument Inc.) was performed on about 45 mg powder samples with a heating rate of 8 °C/min in a flowing high–purity nitrogen stream (100 mL/min); Al_2O_3 powder and Pt were used as reference and material for pan, respectively. Oxygen permeation experiments were performed with sintered disk-shaped specimens with 1.5 mm thickness and 22 mm diameter. They were polished on both sides and then sealed to the end of a quartz-tube with glass sealant at elevated temperatures to form a permeation cell, in which one side of the disk was swept by air at a rate of 100 mL/min and the other side by high–purity helium at a rate of 30 mL/min. Data of each temperature point was taken after a typical equilibration time of 30 min. The composition of the effluent helium stream containing the permeated oxygen was analyzed with a gas chromatograph (HP 6890), and oxygen permeation flux was calculated from the oxygen concentration and rate of the effluent.

Electrical conductivity was measured by a dc four-probe method on bar-shaped samples of a typical dimension of $20 \times 5 \times 2\,mm^3$, using platinum wires attached by Pt paste to samples as probes. Constant current of 10 mA was supplied by a potentiostat/galvanostat Model 263 (Princeton Applied Research), and a multimeter (Keithley 2000) was used to monitor the voltage drop between the inner probes. To follow the synchronous variation in the electrical conductivity with temperature, the data were taken with a dynamic mode, with a heating or cooling rate of 1 °C/min in the temperature range of 450–1050 °C.

3. Results

3.1. Oxygen permeation properties

Fig. 1 depicts the oxygen permeation properties of SCCFO and SCO, which feature abrupt jumps at characteristic regions of temperature for both oxides. At elevated temperatures, the two oxides are all well permeable to oxygen. For example, at 900 °C during the cooling procedure, with 1.5 mm thick SCCFO and SCO membranes, oxygen permeation rates as large as 1.5 and 2.0 mL/min/cm^2 membrane surface area could be attained by applying a relatively small oxygen partial pressure gradient ($p'_{O_2} = 0.21$ atm, $p''_{O_2} = 0.06$ atm), which is slightly higher than those observed for some existing materials, such as $SrCo_{0.8}Fe_{0.2}O_{3-\delta}$ [4,15] and $Ba_{0.5}Sr_{0.5}Co_{0.8}Fe_{0.2}O_{3-\delta}$ [16].

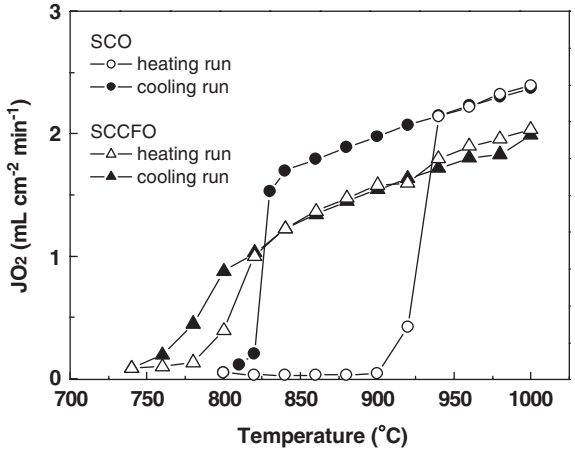

Fig. 1. Temperature dependence of oxygen permeation rates through $Sr_{0.9}Ca_{0.1}Co_{0.89}Fe_{0.11}O_{3-\delta}$ (SCCFO) and $SrCoO_{3-\delta}$ (SCO) membranes with a thickness of 1.5 mm.

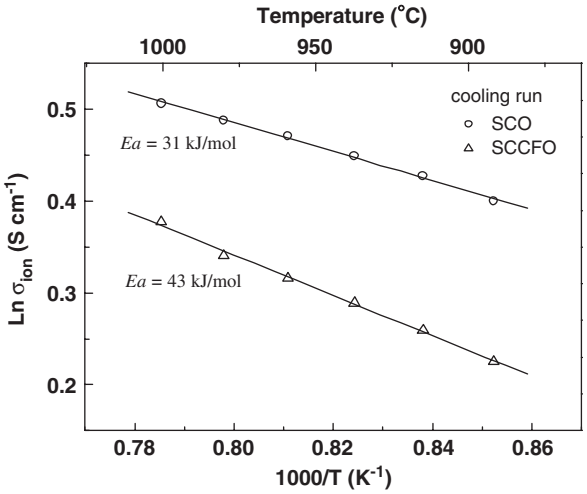

Fig. 2. Arrhenius plots of the variation of oxide–ion conductivity with inverse temperature for $Sr_{0.9}Ca_{0.1}Co_{0.89}Fe_{0.11}O_{3-\delta}$ (SCCFO) and $SrCoO_{3-\delta}$ (SCO).

However, down to characteristic temperatures upon cooling, the oxygen permeability of both oxides diminished sharply to values that is slightly larger than or close to the detection limits of the apparatus (less than 10^{-12} mol cm^{-2} s^{-1}) for SCCFO and SCO, respectively; it could be recovered when the temperature was raised again to a certain value. Moreover, the oxygen permeation of SCO showed a hysteresis as large as about 100 °C, i.e., shifting from ~830 °C on cooling to ~930 °C on heating. In contrast, abrupt changes in oxygen permeability for SCCFO during the cooling and heating procedures occurred at both around ~800 °C.

Using Eq. (2), one can obtain the oxide–ion conductivity for the two oxides. In Fig. 2, data in the temperature range of 1000–880 °C, which are above the abrupt transition during the cooling procedure are shown. Corresponding to the high oxygen permeability, both SCCFO and SCO exhibit markedly large oxide–ion conductivity, which takes values of 1.7 and 2.5 S/cm at 900 °C, respectively. Moreover, the temperature dependence of the ionic conductivity follows the Arrhenius equation with activation energies of 31 and 43 kJ/mol for SCO and SCCFO, respectively. The value for SCCFO is comparable to those observed for $SrCo_{0.8}Fe_{0.2}O_{3-\delta}$ (45 kJ/mol) [15] and $Ba_{0.5}Sr_{0.5}Co_{0.8}Fe_{0.2}O_{3-\delta}$ (41 kJ/mol)[16] over the same temperature range. However, the value for SCO is much lower than their values.

3.2. Electronic transport properties

Fig. 3 shows the variable-temperature measurement results of electrical conductivity for SCCFO and SCO. Notably, similar to the oxygen permeation behaviors, the electrical conductivity of both materials also exhibits abrupt changes around almost same temperature regions. During the cooling procedure, the maximum conductivity obtained for SCCFO and SCO was found to be 200 S/cm at 755 °C and 210 S/cm at 830 °C, respectively, whereas it decreased to values of 90 and 20 S/cm when the temperature was lowered to 650 °C. Considering the fact that the oxide–ion conductivity derived from the oxygen permeability is at least two orders of magnitude lower than it, the conductivity shown in Fig. 3 practically could be taken as the electronic one. Also, as in the case of oxygen permeability, the onset temperature of abrupt changes in the electrical conductivity on cooling and heating for SCCFO was almost coincident with each other, but that for SCO showed a large hysteresis.

It is also worthwhile to note that for both oxides, their electronic conductivity increases as temperature increases until that abrupt change; this trend agrees with a semiconductor behavior. In comparison, their electronic conductivity decreases as temperature increases after that abrupt change; this is characteristic of metallic behavior, indicating a change from semiconductor to metal occurring in these kinds of oxides in the studied temperature range.

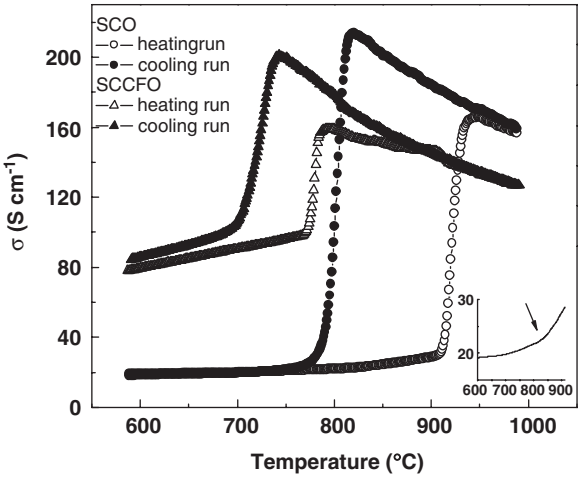

Fig. 3. Temperature dependence of electrical conductivity of $Sr_{0.9}Ca_{0.1}Co_{0.89}Fe_{0.11}O_{3-\delta}$ (SCCFO) and $SrCoO_{3-\delta}$ (SCO) in air.

3.3. Thermal analysis data

DTA and TG data (Fig. 4) show a large endothermic peak centered at ~815 °C and ~930 °C for SCCFO and SCO, respectively, which is coincident with a fairly sharp decrease in weight at the corresponding temperature regions. Moreover, the peak area of SCO is larger than that of SCCFO, indicating much more heat qualities are involved. As for SCO, besides the large endothermic peak at 930 °C, a small endothermic peak, accompanied by a slight weight loss, as also observed with the minimum at ~828 °C.

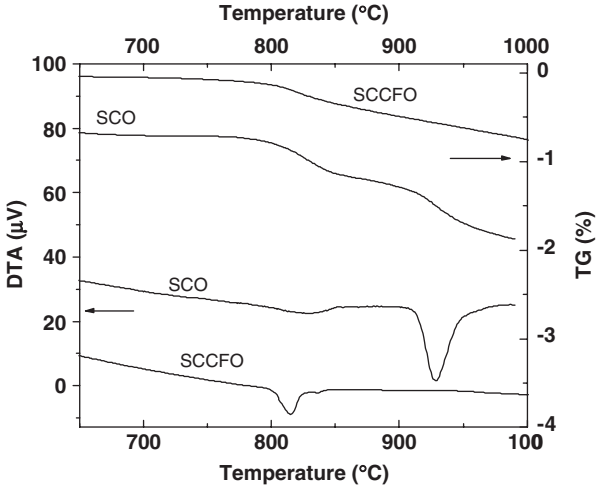

Fig. 4. Differential thermal analysis (DTA) and thermogravimetry (TG) curves of $Sr_{0.9}Ca_{0.1}Co_{0.89}Fe_{0.11}O_{3-\delta}$ (SCCFO) and $SrCoO_{3-\delta}$ (SCO) in N_2.

3.4. High-temperature XRD studies

XRD measurements were performed on SCCFO and SCO in the temperature range from room temperature to 1100 °C in air. Figs. 5 and 6 show the XRD results for SCCFO and SCO, respectively. Obviously, a phase transformation occurred in both SCCFO and SCO during the heating procedure, at about ~800 °C and ~940 °C, respectively. For SCCFO, the XRD patterns above and below the phase transition, e.g., at 1000 and 750 °C, could be readily indexed as a cubic perovskite structure (C, $a = 3.944$ Å) and an orthorhombic brownmillerite structure (B, $a = 5.642$, $b = 15.816$ and $c = 5.497$ Å), which is in good agreement with previous data [19,20].

For SCO, the XRD patterns above the transformation, e.g., at 1000 °C, could also be readily indexed assuming the same cubic perovskite structure (C, $a = 3.952$ Å) as that of SCCFO. Its XRD patterns below the transformation, however, seem to be fairly complex; the one, e.g., at 700 °C could be basically indexed to a hexagonal phase (H, $a = 9.578$ and $c = 12.476$ Å), along with minor amounts of CoO phase and some unknown phases as indicated by several peaks at $2\theta = 47.41$, 55.52°. The XRD patterns of the hexagonal phase are in good agreement with previous results, which is described as being a hexagonal 2H-type structure [9,17].

4. Discussion

It is known that transport of oxide ions in the perovskite–related mixed–conducting oxides, just as in the case of present materials, mostly proceeds via jumping of oxygen vacancies, and electrons transport along the $B^{n+} - O^{2-} - B^{(n-1)+}$ network owing to the overlapping of

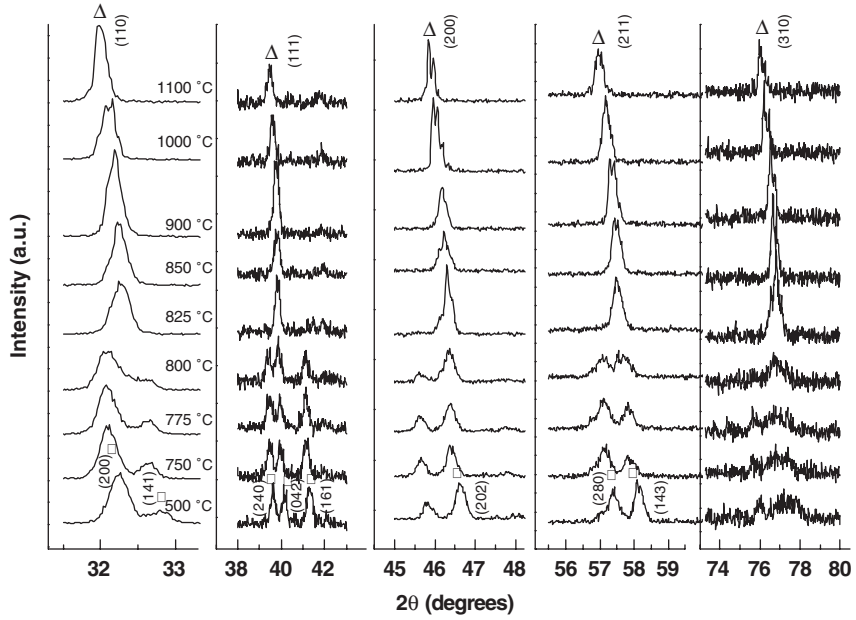

Fig. 5. Variable-temperature X-ray diffraction patterns of $Sr_{0.9}Ca_{0.1}Co_{0.89}Fe_{0.11}O_{3-\delta}$ (SCCFO) in air atmosphere. Peaks denoted by (□) and (Δ) could be indexed as an orthorhombic brownmillerite and a cubic perovskite structure, respectively.

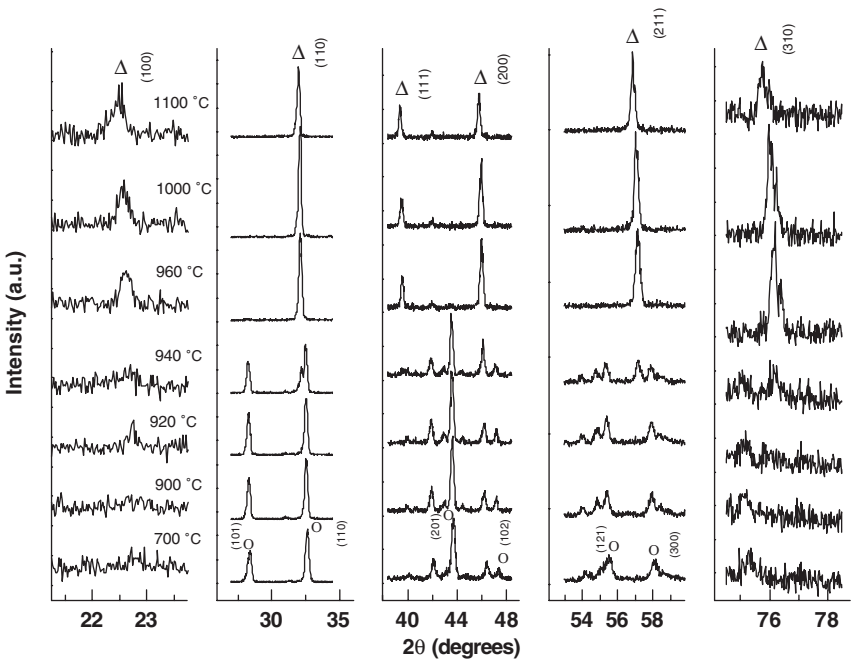

Fig. 6. Variable-temperature X-ray diffraction patterns of $SrCoO_{3-\delta}$ (SCO) in air atmosphere. Peaks denoted by (○) and (Δ) could be indexed as a hexagonal and a cubic perovskite structure, respectively.

oxygen's *p* orbital and transitional metal's *d* orbital. Among those factors that have impact on the transport of oxide ions, the distribution state of oxygen vacancies plays a crucial role. As evidenced by high-temperature XRD analysis (Fig. 5), the SCCFO system adopts an orthorhombic brownmillerite structure (B) and a cubic perovskite one (C) below and above the phase transformation, which relation is schematically illustrated in Fig. 7a and c. As shown, the brownmillerite structure features an ordered distribution of oxygen vacancies along the $[101]_p$ direction in alternating $(0k0)$ perovskite planes, which has long been found in several systems including Ca_2AlFeO_5 [18], $Ba_2In_2O_5$[14], and $SrCo_{0.80}Fe_{0.20}O_{3-\delta}$ (Fig. 7a) [19,20]. In such a structure, oxide ions are immobile owing to the ordering and pinning states of the oxygen vacancies. With the increase in temperature, oxide ions can transport, but only in a confined two-dimensional *ac* plane. Further increment of temperature will make oxygen vacancies randomly distributed and completely mobile, which is vital to the three-dimensional transport of oxide ions. Together with the order–disorder of oxygen vacancies, a structural transformation from brownmillerite to cubic perovskite occurs. Meanwhile, the cubic structure is also ideal for the transport of electrons as the cubic symmetry leads to higher magnitude of overlapping of oxygen's 2*p* orbital and transitional metal's 3*d* orbital, even to maximum for the B–O–B bond with an angle of 180° in an ideal cubic lattice (Fig. 7c). During a cooling procedure, a reverse process to that described above could take place. Corresponding to the phase transformations, the oxygen permeability and

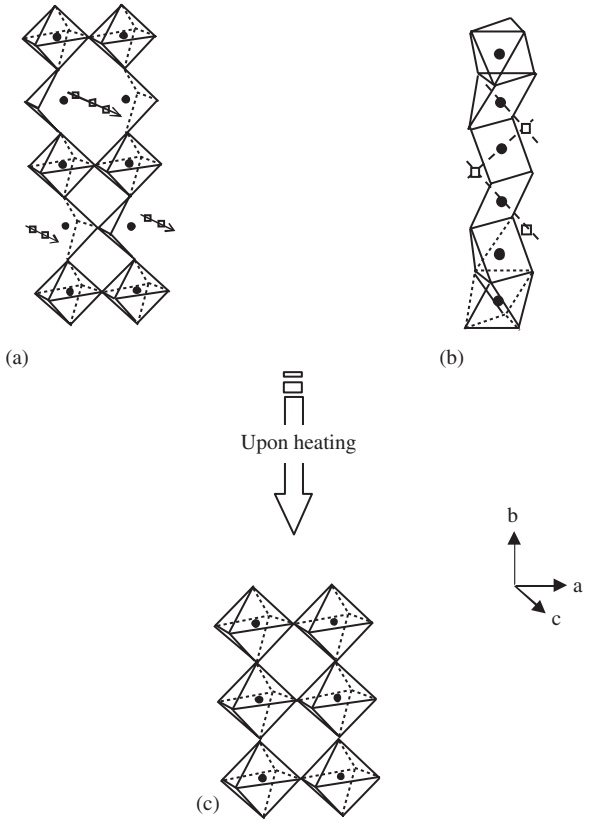

Fig. 7. The schematic structures of the low-temperature orthorhombic brownmillerite $Sr_{0.9}Ca_{0.1}Co_{0.89}Fe_{0.11}O_{3-\delta}$ (SCCFO) and hexagonal $SrCoO_{3-\delta}$ (SCO), and their high-temperature cubic perovskite structure. (□) represent the oxygen vacancies.

electrical conductivity of the present materials showed abrupt jumps versus the temperature. Such reversible jumps in transport properties have also been found in many oxide–ion conductors such as Bi_2O_3 [21], $La_2Mo_2O_9$[22], and $Ba_2In_2O_5$ [13,14], which were believed to correspond to an order–disorder transition on the oxygen sublattice, associated with a reorganization of the cationic sublattice [17]. The same process is expected to also occur in the present materials.

Despite that SCO has a similar cubic perovskite phase as that of SCCFO system at high temperatures, SCO adopts a different crystal structure at low temperatures (see Fig. 6). The crystallographic structures of SCO system have been the subject of several investigations [9,17,23,24]. It was known to assume a number of phases, e.g., hexagonal 2H-type form, cubic perovskite, and orthorhombic or rhombohedral brownmillerite, depending on the annealing temperature and atmosphere. It was also found that phase separation and microdomain formation tend to occur in the SCO system during cooling down to room temperature [23,25]. In the present study, the XRD patterns of SCO at low temperatures, e.g., from 700 °C through 940 °C, reveal the samples consist of mainly the hexagonal 2H-SCO phase, which is characterized by the chains of face-shared BO_6 octahedron run parallel to the *b*-axis with *A* site cations being distributed between the chains [9] and the vacancy-ordered state [17] (as shown in Fig. 7b). Accordingly, the conduction for both oxide–ions and electrons in such a structure is confined in quasi-one dimension along the *b*-axis at low temperatures. When raising the temperature to a critical value, concomitant with the phase transformation from a hexagonal structure to a cubic one, the oxygen permeability and electrical conductivity of SCO increased sharply at the transition as that of SCCFO. Harrison et al. determined the room-temperature phase of SCO as $Sr_6Co_5O_{15}$ along with a negligible amount of Co_3O_4 by neutron diffraction analysis [25]. Such an $A_6B_5O_{15}$ structure can also be described by the same hexagonal symmetry, but the chain of polyhedra formed by the alternate face-shared octahedron and triangular prism, unlike that of 2H-ABO_3 formed solely by the face-shared octahedron [26]. Combining with the present results, it is likely that a conversion between the $A_6B_5O_{15}$ phase and the 2H-ABO_3 phase may occur in the SCO system at low temperatures, which will be discussed later. Additionally, it seems to be a common inclination for Co-containing perovskite-type oxides, e.g., SCO and $BaCoO_{3-\delta}$ [27], to adopt vacancy-ordered structures, due to a high concentration of oxygen-vacancy formation facility in them. Furthermore, vacancy-ordering in these oxides may assume diverse kinds of configurations [28,29]. In order to discern the specific ordering structures in these materials, further microscopic analyses such as TEM, HRTEM, and *Mössbauer* spectroscopy are desired and will be conducted in future.

Phase transformations occurring in both SCO and SCCFO systems were also confirmed by the DTA-TG results, which show endothermic peaks at the related region of temperature (Fig. 4). Moreover, endothermic peaks in both oxides were coupled with fairly sharp oxygen release. The same phenomenon was also found in the $SrCo_{0.80}Fe_{0.20}O_{3-\delta}$ [10] and $Sr_{0.9}Ca_{0.1}CoO_{3-\delta}$ [11] systems, indicating that this kind of phase transformation may be induced by the oxygen desorption from the lattice. It is known that in the present materials holes are the majority carriers [3,15], the oxygen loss from materials is expected to result in a decrease in the carriers' concentration and thus the conductivity as described in Kroger-Vink notation

$$2B_B^{\bullet} + O_O^{\times} \rightarrow V_O^{\bullet\bullet} + B_B^{\times} + 1/2O_2(g). \quad (3)$$

And this is the case at higher temperatures for the two materials (see Fig. 3), where their electronic conductivity decreases as temperature decreases. On the contrary, their conductivity increases with increasing temperature at low temperatures, which may result from the increasing carrier mobility with increasing temperature, despite a small amount of oxygen loss at this temperature range. At these characteristic temperatures, the electrical conductivity for both SCO and SCCFO increases sharply while a significant amount of oxygen is released (Figs. 1 and 4). Obviously, the abrupt conductivity change is related directly with the phase transformation occurring in these two materials, as described above. As for this minor endothermic peak at around ~828 °C in SCO, it cannot be identified definitely at this moment, but it may be associated with the conversion of $Sr_6Co_5O_{15}$ into SCO. Electrical measurement results also support this hypothesis, which reveal an obvious increase at the same temperature range (see inset in Fig. 3). This conversion, however, cannot be recognized by the X-ray diffraction data, which show no detectable changes on those patterns collected between 700 and 940 °C (Fig. 6), suggesting the close relation between the two phases. A similar phenomenon was also observed in the multiphase $SrFeCo_{0.5}O_y$ system, which may be an indication of change in the phase composition [8]. Note that phase transformation temperature of the two materials revealed by DTA is slightly different from those of the oxygen permeability and electrical conductivity measurements; this probably could be attributed to the different heating rates applied by different measurements.

As shown above, the relation between the present three structures, the orthorhombic brownmillerite structure (B), the hexagonal 2H-type structure (H) and the cubic perovskite (C) is clear. Their crystal symmetry increases in the following order: H < B < C. The brownmillerite structure is closely related to the perovskite one; they only differ by the oxygen vacancy distribution. The hexagonal 2H-type structure; however, has a different stacking sequence of cations from those of the other two. Therefore, the hexagonal phase of SCO exhibits lower oxygen permeability and electrical conductivity than that of the brownmillerite structure in SCCFO at low temperatures, due to its lower lattice symmetry than that of brownmillerite (Figs. 1 and 2). Meanwhile, the *H*/*C* transformation

needs to absorb much more heat quantity and occur at a higher temperature than that of the B/C transformation (Fig. 4), because this transformation involves both the order–disorder transition of oxygen vacancies and the long-range reorganization of cations, whereas the latter mainly involves the order–disorder transition of oxygen vacancies and/or, if any, slight deformation of cations. Another point of note is that, contrary to the cases of low temperatures, the oxygen permeability and electrical conductivity of the SCO above the transition are slightly higher than that of the SCCFO system, in spite of the same cubic perovskite structure being adopted by both oxides. This can be interpreted from the nature difference between Co and Fe elements, since Co is believed to have a relatively weaker bond with oxide–ion and higher ability to fluctuate between different valances than Fe [3,8].

As shown above, the low-temperature stable phase of SCO is that of hexagonal 2H-type structure, which may be stabilized by a maximum metal–metal interaction between face-shared CoO_6 octahedrons (see Fig. 7b) [30]. Formation of such a structure is induced by the mismatch of the equilibrium (Sr–O) and (Co–O) bond lengths that gives a geometric tolerance factor:

$$t \equiv (\mathrm{Sr}-\mathrm{O})/\sqrt{2}(\mathrm{Co}-\mathrm{O}) > 1. \quad (4)$$

Reduction of t is expected to convert the stacking of SrO_3 plane from a hexagonal sequence to a cubic one, which can be achieved by decreasing the (Sr–O) and/or increasing the (Co–O) bond lengths [31]. As demonstrated in the present study, one way to decrease t is to simultaneously substitute Sr by smaller Ca with 10 mol% and Co by slightly larger Fe with 11 mol%, resulting in a transformation from the hexagonal 2H-related structure (H) to the orthorhombic brownmillerite structure (B). Another alternative way to decrease t is to extract oxygen, thereby reducing some of Co(IV) to Co(III) and increasing the (Co–O) bond lengths; this is the case that at elevated characteristic temperatures a transformation from an H or B structure to a cubic structure (C) occurs. As demonstrated in this study, since the 2H-type structure is the low-temperature stable form of SCO system, it will transform into the cubic perovskite structure at elevated temperature, without forming the brownmillerite phase under the present measurements condition, thus making it impossible to probe the influence of B–C transformation on the transport properties. In contrast, the selected SCCFO system adopts a B structure in the whole low–temperature range until it transforms to a C structure. It is of significance to illustrate the relationship between the transport properties and B–C transformation, especially which is likely related the order–disorder transition of oxygen vacancies in mixed–conducting oxides.

5. Conclusions

Based on two typical model systems, $Sr_{0.9}Ca_{0.1}Co_{0.89}Fe_{0.11}O_{3-\delta}$ (SCCFO) and $SrCoO_{3-\delta}$ (SCO), the correlation between transport properties and phase transformation in mixed-conducting oxides has been well revealed. Remarkably high oxygen permeability and electrical conductivity at high temperatures have been verified for the two materials. At 900 °C for example, 1.5-mm-thick SCCFO and SCO membranes remarkably showed oxygen rates as large as 1.5 and 2.0 mL/min/cm^2, respectively. When cooled down to certain characteristic temperatures, their oxygen permeation properties were lost, which could be recovered by increasing the temperature again to certain values. Similar trends to those for oxygen permeability were also observed on electrical conductivity around the same regions of temperature. A phase transformation between a low-temperature orthorhombic brownmillerite structure (B) or a hexagonal 2H-type structure (H) and a high-temperature cubic perovskite structure (C) occurring in SCCFO and SCO, respectively, is responsible for the abrupt change in transport properties. Moreover, the present phase transformations are perhaps directly associated with the order–disorder transition of oxygen vacancies. Compared with the B/C transition, the H/C transition occurs at higher temperatures and adsorbs more heat quantity, since that process necessarily involves both the cooperative long-range reconstruction of cations and order–disorder transition of oxygen vacancies.

References

[1] H.J.M. Bouwmeester, A.J. Burggraaf, in: A.J. Burggraaf, L. Cot (Eds.), Fundamentals of Inorganic Membrane Science and Technology, Elsevier, Amsterdam, 1996.
[2] C. Zener, Phys. Rev. 82 (1952) 403.
[3] L.W. Tai, M.M. Nasrallah, H.U. Anderson, D.M. Sparlin, S.R. Sehlin, Solid State Ionics 76 (1995) 259.
[4] Y. Teraoka, H.M. Zhang, S. Funrukawa, N. Yamazoe, Chem. Lett. (1985) 1743.
[5] U. Balachandran, J.T. Dusek, P.S. Maiya, B. Ma, R.L. Mieville, M.S. Kleefisch, C.A. Udovich, Catal. Today 36 (1997) 265.
[6] Z.Q. Deng, W. Liu, C.S. Chen, H. Lu, W.S. Yang, Solid State Ionics 170 (2004) 187.
[7] J.E. Elshof, Dense inorganic membranes — Studies on transport properties, defect chemistry and catalytic behavior, Ph.D. Dissertation, University of Twente, Netherlands, 1997.
[8] Z.Q. Deng, G.G. Zhang, W. Liu, D.K. Peng, C.S. Chen, Solid State Ionics 152–153 (2002) 735.
[9] Y. Takeda, R. Kanno, T. Takeda, O. Yamamoto, Z. Anorg. Allg. Chem. 540–541 (1986) 259.
[10] H. Kruidhof, H.J.M. Bouwmeester, R.H.E.V. Doorn, A.J. Burggraaf, Solid State Ionics 63 (1993) 816.
[11] N. Miura, H. Murae, H. Kusaba, J. Tamaki, G. Sakai, N. Yamazoe, J. Electrochem. Soc. 146 (1999) 2581.
[12] J.B. Goodenough, A. Manthiram, P. Paranthaman, Y.S. Zhen, Solid State Ionics 52 (1992) 105.
[13] S.B. Adler, S. Russek, J. Reimer, M. Fendorf, A. Stacy, Q. Huang, A. Santoro, J. Lynn, J. Baltisberger, U. Werner, Solid State Ionics 68 (1994) 193.
[14] M. Yoshinaga, M. Yamaguchi, T. Furuya, S.R. Wang, T. Hashimoto, Solid State Ionics 169 (2004) 9.
[15] Z.Q. Deng, Preparation and oxygen transport properties of $SrFe_{1.5}O_y$ and $SrCoO_{3-\delta}$-based membrane materials, Ph.D. Dissertation, University of Science and Technology of China, PR China, 2002.

[16] Z.P. Shao, W.S. Yang, Y. Cong, H. Dong, J.H. Tong, G.X. Xiong, J. Membr. Sci. 172 (2000) 177.
[17] J.C. Grenier, L. Fournes, M. Pouchard, P. Hagenmuller, Mater. Res. Bull. 21 (1986) 441.
[18] A.A. Colville, S. Geller, Acta Crystallogr. 27 (1971) 2311.
[19] L.M. Liu, T.H. Lee, L. Qiu, Y.L. Yang, A.J. Jacobson, Mater. Res. Bull. 31 (1996) 29.
[20] F. Prado, N. Grunbaum, A. Caneiro, A. Manthiram, Solid State Ionics 167 (2004) 147.
[21] H.A. Harwig, A.G. Gerards, J. Solid State Chem. 26 (1978) 265.
[22] P. Lacorre, F. Goutenoire, O. Bohnke, R. Retoux, Y. Laligant, Nature 404 (2000) 856.
[23] S. Stemmer, A. Sane, N.D. Browning, T.J. Mazanec, Solid State Ionics 130 (2000) 71.
[24] J. Rodringuez, J.M. Gonzalez-Calbet, Mater. Res. Bull. 21 (1986) 429.
[25] W.T.A. Harrison, S.L. Hegwood, A.J. Jacobson, J. Chem. Soc., Chem. Commun. (1995) 1953–1954.
[26] K. Boulahya, M. Parras, J.M. Gonzalez-Calbet, J. Solid State Chem. 145 (1998) 116.
[27] A. Varela, M. Parras, K. Boulahya, J.M. Gonzalez-Calbet, J. Solid State Chem. 128 (1997) 130.
[28] A.I. Becerro, F. Langenhorst, R.J. Angel, S. Marion, C.A. McCammon, F. Seifert, Phys. Chem. Chem. Phys. 2 (2000) 3933.
[29] Y. Takeda, K. Kanno, T. Takada, O. Yanamoto, J. Solid State Chem. 63 (1986) 237.
[30] T. Negas, R.S. Roth, J. Solid State Chem. 1 (1970) 409.
[31] R.S. Tichy, J.B. Goodenough, Solid State Sci. 4 (2002) 661.